catalysts

MDPI

Article

Photoelectrocatalytic vs. Photocatalytic Degradation of Organic Water Born Pollutants

Ioannis Papagiannis [1], Georgia Koutsikou [2], Zacharias Frontistis [3], Ioannis Konstantinou [2], George Avgouropoulos [1], Dionissios Mantzavinos [3] and Panagiotis Lianos [3,*]

1 Department of Materials Science, University of Patras, 26500 Patras, Greece; giannis489@gmail.com (I.P.); geoavg@upatras.gr (G.A.)
2 Department of Chemistry, University of Ioannina, 45110 Ioannina, Greece; ch04507@cc.uoi.gr (G.K.); iokonst@cc.uoi.gr (I.K.)
3 Department of Chemical Engineering, University of Patras, 26500 Patras, Greece; zaxoys@gmail.com (Z.F.); mantzavinos@chemeng.upatras.gr (D.M.)
* Correspondence: lianos@upatras.gr; Tel.: +30-26-1099-7513

Received: 7 September 2018; Accepted: 10 October 2018; Published: 15 October 2018



Abstract: The azo dye Basic Blue 41 was subjected to photocatalytic and photoelectrocatalytic degradation using nanopararticulate titania films deposited on either glass slides or Fluorine doped Tin Oxide (FTO) transparent electrodes. The degradation was carried out by irradiating titania films with weak ultraviolet (UVA) radiation. The degradation was faster when using FTO as a titania support even without bias and was further accelerated under forward electric bias. This result was explained by enhanced electron-hole separation even in the case of the unbiased titania/FTO combination. This system for organic material photocatalytic degradation was also successfully applied to the degradation of the anti-inflammatory drug piroxicam, which demonstrated a well distinguished degradation behavior in going from a plain glass support to unbiased and biased FTO. The degradation pathway of piroxicam has been additionally studied using liquid chromatography-accurate mass spectrometry analysis.

Keywords: photocatalytic degradation; photoelectrocatalytic degradation; Basic Blue 41; piroxicam

1. Introduction

It is generally accepted that photoelectrocatalytic treatment of organic pollutants can accelerate their photocatalytic degradation [1–5]. In a photoelectrocatalytic system, a mesoporous photocatalyst is usually deposited on the anode electrode. By applying a forward bias, that is, by applying a positive polarization on the photoanode, electrons are removed thus facilitating electron-hole separation. Higher electron-hole separation is always translated into higher photocatalytic efficiency, particularly in what concerns photocatalytic oxidation. Various photocatalysts have been tested for photoelectrocatalysis, however, titania occupies the most prominent position. In most of the recently published works, researchers opt for the employment of titania nanotube photoanodes, formed by anodization on titanium sheets or titanium grids, since such electrodes have a large capacity for adsorbing organic material [1–3,6,7]. Adsorption of organic molecules on the photocatalyst obviously facilitates photocatalytic oxidation by direct electron donation from the organic agent to the semiconductor [8]. A disadvantage of titania nanotubes is that they form an opaque electrode. For this reason, many researchers prefer to use mesoporous nanocrystalline titania films deposited on transparent electrodes, typically Fluorine doped Tin Oxide (FTO) [3]. Such electrodes are very easy to make, they are stable and they are convenient to use with all kinds of reactor and light-source configuration. In addition and as will be discussed below, FTO electrochemical potential is convenient

for transfer of electrons from titania, thus facilitating electron-hole separation. In the present work we have also chosen to employ photoanodes made by depositing mesoporous nanoparticulate titania on FTO electrodes.

Among water-born organic pollutants that have attracted the interest of researchers, dyes and pharmaceutical compounds receive the greatest attention [3–7,9–13]. Both are extensively used, the former in the textile and leather industry, while the latter are consumed as drugs for humans and animals. Their extensive use has resulted in the release of large quantities into the aquatic environment. These pollutants are resistant to biological treatment, therefore, Advanced Oxidation Processes (AOPs) are necessary to degrade dyes and pharmaceutical products. Among various AOPs, photocatalytic degradation is the most popular and effective means to degrade recalcitrant pollutants. In the present work, we have chosen a typical dye, Basic Blue 41, and a popular drug, Piroxicam (PRX), to test the ability of a simple photoelectrocatalytic system to degrade these products. Photoelectrocatalytic has been compared with photocatalytic degradation in order to highlight the potential of the former to accelerate degradation rate.

Basic Blue 41 (BB41) is an azo-dye (see Figure 1 for its chemical structure), which has been frequently used as a model dye to test photocatalytic degradation [14–17]. It has also been used in the present work as a model dye to study photoelectrocatalytic vs. photocatalytic degradation. The obtained results then served as a guide to study piroxicam photocatalytic and photoelectrocatalytic degradation under similar conditions. Piroxicam is a nonsteroidal anti-inflammatory drug (see Figure 1 for its chemical structure). Degradation of water born piroxicam has, to our knowledge, never been studied by photocatalysis and there are not many works related to AOP treatment of this drug. Thus, a recent work [18] employed sonochemical oxidation to study its degradation. Anti-inflammatory drugs are very popular in modern societies, because they are used to relieve pain. Owing to their broad use, they are detected in the aquatic environment causing major concern since they present a serious danger for the biological systems even at trace amounts [19,20]. For this reason, the present data offer an alternative route for effective water treatment and reuse.

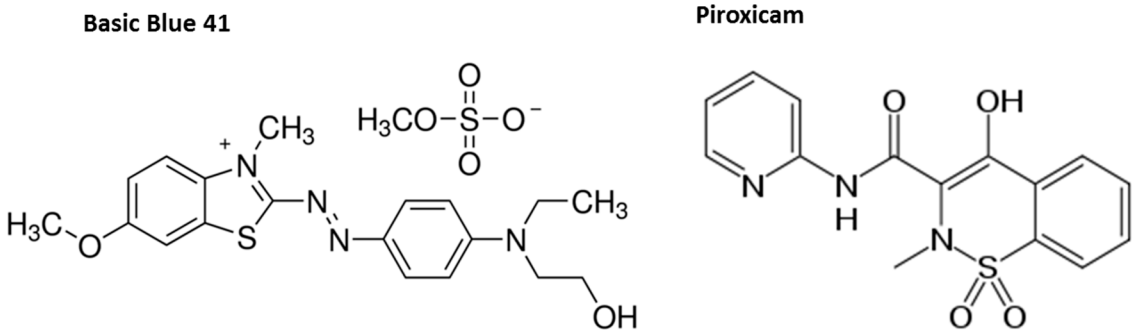


Figure 1. Chemical structure of Basic Blue 41 (BB41) and Piroxicam.

2. Results and Discussion

Photocatalytic and photoelectrocatalytic degradation of both BB41 and piroxicam were carried out in a cylindrical batch reactor made of pyrex glass capable of accommodating a photoanode, counter, and reference electrode. Details are provided in Section 3.3.

2.1. Photocatalytic and Photoelectrocatalytic Degradation of BB41

As explained in the Introduction, BB41 was used as a model dye to study photoelectrocatalytic vs. photocatalytic degradation. Aqueous solutions of 2×10^{-5} M (~10 ppm) BB41 have been employed and the decoloration of the solution was monitored by absorption spectrophotometry at 608 nm, as seen in Figure 2. This concentration was chosen in order to obtain sufficient absorbance whilst being low enough to avoid light obstruction. The curves of Figure 3 have been drawn, according to the common practice, by assuming that the peak absorbance is proportional to the concentration

of the intact dye in solution. In Figure 3, there are five curves. Curve (1) shows dye degradation under purely photocatalytic conditions. The photocatalyst was supported on a glass slide and it was immerged in the dye aqueous solution without any electrolyte. After 23 h of weak black-light irradiation under the above described conditions, dye decolorization reached 83%. However, when the photocatalyst was supported on an FTO glass under identical conditions, the decoloration was faster (86% after 23 h, Curve 2) and became even faster when 0.5 M Na_2SO_4 was added to the aqueous solution (88% after 23 h, Curve 3). These differences are relatively small but they are reproducible with less than 1% error. As is shown below, they were much more pronounced in the case of piroxicam. When FTO with photocatalyst was used as working electrode in a 3-electrode configuration, application of a forward (positive) bias further accelerated degradation. Thus, by applying a bias of +1 V vs. Ag/AgCl, after 23 h the decoloration reached 95% (Curve 4). Finally, by applying a reverse bias of −1 V vs. Ag/AgCl, decoloration was slowed down so that after 23 h only 76% of the dye was destroyed.

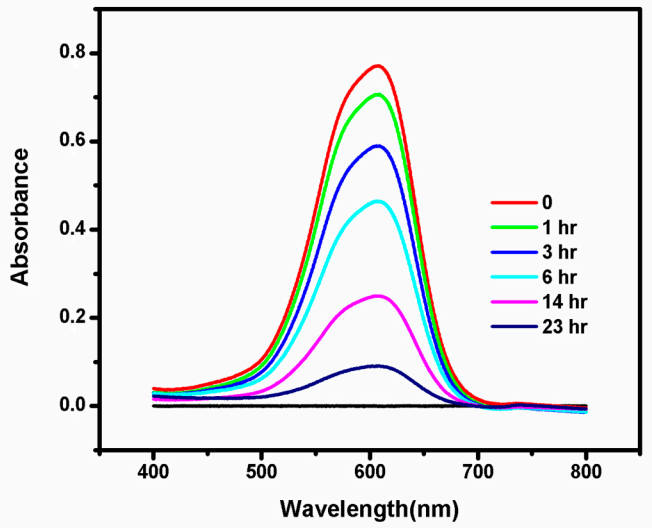


Figure 2. Variation of the absorption spectrum of 2×10^{-5} M (~10 ppm) aqueous solution of BB41 by photocatalytic degradation in the presence of a titania film supported on Fluorine doped Tin Oxide (FTO) glass under black-light radiation.

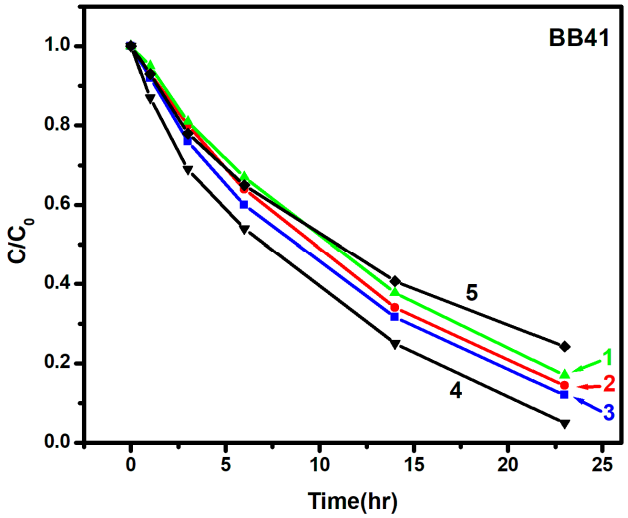


Figure 3. Degradation curves for BB41 for various types of photocatalyst supports and operation conditions: (**1**) plain glass slide; (**2**) FTO; (**3**) FTO plus supporting electrolyte without electric bias; (**4**) +1 V bias vs. Ag/AgCl; and (**5**) −1 V bias vs Ag/AgCl.

The acceleration of discoloration, albeit small, in going from a plain glass to an FTO glass is an interesting observation. As will be seen below, the difference becomes larger in the case of piroxicam. We believe that it is due to transfer of electrons from titania photocatalyst to FTO. The conduction band level of titania is about 0.2 V more negative than the energy level of FTO [21], therefore, it favors unassisted photo-generated electron injection from titania to FTO, which works in favor of electron-hole separation. The oxidative power of holes is then enhanced while electrons may diffuse along FTO and may participate in reduction reactions, for example, $^{\bullet}O_2^-$ radical formation, which may add to photocatalytic degradation. This is the basis of operation of a "photocatalytic leaf", which has been used in the past for unassisted hydrogen production by water reduction [22]. This operation is facilitated in the presence of a supporting electrolyte, thus it explains why addition of Na_2SO_4 presently further enhanced discoloration.

Application of forward bias, as expected, substantially accelerated dye discoloration by enhancing electron-hole separation and thus enhancing the oxidative power of the photo-generated holes. BB41 is a positively charged dye, which is expected to be repelled by a positively charged electrode. This would in principle reduce direct oxidation, since direct electron transfer from the dye to the semiconductor would then become less probable. If then the degradation rate is accelerated despite the repelling electric polarization, another degradation mechanism must prevail. It is thus concluded that the formation of reactive radicals, either through the $OH^- + h^+ \rightarrow {}^{\bullet}OH$ or the $SO_4^{2-} + h^+ \rightarrow {}^{\bullet}SO_4^-$ reaction must be the prevalent oxidation route. Consequently, the discoloration rate was extensively reduced when a reverse bias was applied, despite the fact that in that case, the attraction of positively charged dye molecules is enhanced.

As a conclusion to this section, it has been shown that when titania photocatalyst is deposited on an unbiased FTO electrode, the degradation is enhanced compared to that obtained with titania deposited on plain glass. The degradation is further enhanced by applying a forward bias. This concrete model was then applied to the degradation of piroxicam, as discussed in the following section.

2.2. Photocatalytic and Photoelectrocatalytic Degradation of Piroxicam

Piroxicam was photocatalytically degraded under similar conditions as BB41 and the results are presented in Figures 4 and 5. The concentration of piroxicam was 40 ppm. This material is hardly soluble in water. In order to facilitate its solubilization, highly-concentrated piroxicam was first dissolved in acetonitrile and then transferred to an aqueous solution. Thus, aqueous solutions of piroxicam always contained a small quantity of acetonitrile. Degradation of piroxicam was first monitored by its UV-Vis spectra peaking around 365 nm (cf Figure 4). When titania was deposited on plain glass, photocatalytic degradation was relatively slow. Only 52% of this material was degraded after 22 h (Curve 1). However, when titania was deposited on unbiased FTO in the presence of a 0.5 M Na_2SO_4 supporting electrolyte, a dramatic acceleration of the degradation rate was obtained leading to about 70% degradation in the same period of time (Curve 2). The degradation was even faster under forward bias reaching more than 88%, again in the same period of time (Curve 3). The model of Section 2.1 is then even better verified by the data of Figure 5.

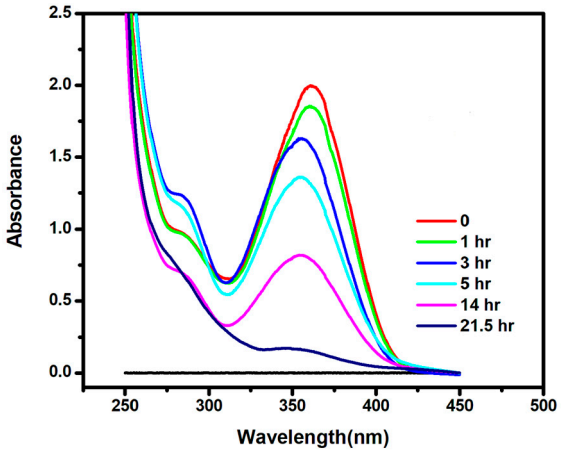


Figure 4. Variation of the absorption spectrum of 40 ppm aqueous solution of piroxicam by photocatalytic degradation in the presence of a titania film supported on FTO glass under black-light radiation.

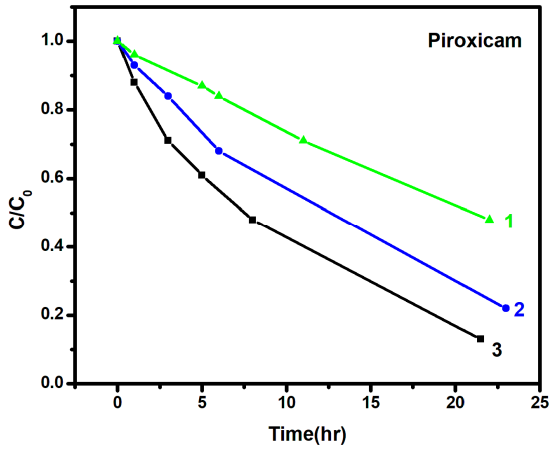


Figure 5. Degradation curves for piroxicam for various types of photocatalyst supports and operation conditions: (**1**) plain glass slide; (**2**) FTO plus supporting electrolyte without electric bias; and (**3**) +1 V bias.

The degradation data for piroxicam support the above presented model. Deposition of the photocatalyst on an FTO electrode accelerates photodegradation, in particular, in the presence of a supporting electrolyte. Thus, FTO with photocatalyst functions as an unassisted photoelectrochemical installation. Degradation is further enhanced by applying a forward bias.

Decrease of the absorption peak does not, of course, mean complete mineralization. Since measurements using UV/VIS spectrophotomerer detect also the oxidation byproducts that absorb at the same wavelength, piroxicam degradation was also studied by using high performance liquid chromatography (HPLC) in two photocatalytically degraded samples with unbiased and biased FTO carrying titania photocatalyst. A removal of 75% and 95% of piroxicam was detected in the two cases, respectively, after 22 h of degradation. It is therefore verified that a forward biased electrode did result in a higher degradation.

2.3. Identification of Degradation Products of Piroxicam and Tentative Decomposition Pathways

Piroxicam has not been previously studied by photocatalysis; therefore, we have proceeded to the analysis of its degradation products by LC-MS chromatography. The identification of piroxicam (PRX) degradation products (DPs) was based on high-resolution accurate mass measurements (UPLC-MS/MS-LTQ-Orbitrap) in negative ionization mode (Table 1). The formation of eight DPs was revealed during photocatalysis. Parent compound PRX presented a molecular ion peak $[M\text{-}H]^-$ at m/z 330.0547, a fragment at m/z 266.0930 was assigned to the loss of -SO_2 following intramolecular rearrangement and the m/z 210.0224

and 146.0615 fragments corresponding to the loss of pyridinecarboxamide moiety and the loss of -SO_2, again following intramolecular rearrangement from the former fragment ion, respectively. Three DPs (DP5, DP6, and DP8) with molecular ions [M-H]$^-$ at m/z 346.0491–346.0495 that differed by about 16 amu from PRX were identified as hydroxylated derivatives. Pyridine, benzothiazine moieties, and the N-methyl group can be considered as potential sites of hydroxylation. DP6 showed MS^2 m/z ions at 251.9960, 226.0171 which corresponded to the loss of amino pyridine and the pyridinecarboxamide moiety, respectively, indicating that the hydroxylation took place at the benzothiazine moiety or the N-methyl group. On the other hand, DP5 showed m/z diagnostic MS^2 m/z ions at 282.0872 and 253.0280 indicating the loss of -SO_2 and C_5H_3NO fragments suggesting the hydroxylation of the pyridinyl ring. Finally, DP8 presented m/z fragment ions at 226.0171 and 162.0565 (loss of -$C_6H_4N_2O$ and -$C_6H_4N_2$-SO_2) suggesting also the hydroxylation of the benzothiazine moiety.

Table 1. High-resolution accurate LC-MS data for piroxicam (PRX) and identified degradation products (DPs) in negative ionization mode.

DP Code	R_t (Min)	Deprotonated Molecular Formula	m/z [M-H]$^-$	Δ (ppm)	RDBE	MS^2 m/z [M-H]$^-$	Deprotonated Molecular Formula	Δ (ppm)	RDBE [+]
DP1	3.18	$C_7H_8NO_2S$	170.0282	0.338	4.5	106.067	C_7H_8N	7.706	4.5
DP2	4.76	$C_8H_6NO_4S$	212.0021	−1.14	6.5				
DP3	6.85	$C_8H_6NO_4S$	212.0019	−1.800	6.5				
		$C_8H_6NO_2$	148.0407	1.947	6.5				
DP4	7.25	$C_8H_6NO_4S$	212.0017	−2.744	6.5				
DP5	8.12	$C_{15}H_{12}N_3O_5S$	346.0493	3.0	11.5	282.0872	$C_{15}H_{12}N_3O_3$	−4.235	11.5
		$C_{15}H_{12}N_3O_3$	282.0872	−4.235	11.5	253.0280	$C_{10}H_9O_4N_2S$	−3.441	7.5
		$C_{10}H_9N_2O_4S$	253.0282	−2.493	7.5				
DP6	8.29	$C_{15}H_{12}N_3O_5S$	346.0491	−3.596	11.5	282.0876	$C_{15}H_{12}N_3O_3$	−2.817	11.5
		$C_{15}H_{12}N_3O_3$	282.0875	−6.504	11.5	251.996	$C_{10}H_6O_5NS$	−2.565	8.5
		$C_{10}H_6O_5NS$	251.9963	−3.596	8.5	226.0171	$C_9H_8NO_4S$	−3.813	6.5
						182.9757	$C_7H_3O_4S$	−0.506	6.5
PRX	8.56	$C_{15}H_{12}N_3O_4S$	330.0547	−2.242	11.5	266.0932	$C_{15}H_{12}N_3O_2$	−1.127	11.5
		$C_{15}H_{12}N_3O_2$	266.0930	−1.916	11.5	210.0227	$C_9H_8O_3NS$	−1.796	6.5
		$C_9H_8NO_3S$	210.0224	−2.796	6.5	169.9966	$C_7H_5O_3S$	0.544	5.5
		C_9H_8NO	146.0615	2.347	6.5				
DP7	9.42	$C_{16}H_{14}N_3O_4S$	344.0703	−2.063	11.5	160.0771	$C_{10}H_{10}NO$	2.266	6.5
		$C_{16}H_{12}N_3O_2$	280.1086	−2.035	11.5	280.1087	$C_{16}H_{14}O_2N_3$	−1.607	11.5
		$C_{10}H_{10}NO_3S$	224.0383	−1.862	6.5	224.0384	$C_{10}H_{10}NO_3S$	−1.103	6.5
		$C_{10}H_{10}NO$	160.0771	2.266	6.5	169.9968	$C_7H_5O_3S$	2.083	5.5
DP8	9.91	$C_{15}H_{12}N_3O_4S$	346.0495	−2.238	11.5				
		$C_9H_8N_3O_2$	226.0174	−2.485	6.5				
		$C_9H_8NO_2$	162.0565	2.765	6.5				
		$C_8H_5NO_2$	147.0328	1.654	7.0				

[+] ring-double bond equivalents.

Three isomeric DPs (DP2, DP3, DP4) with m/z 212.0017–212.0021 are proposed as the mono-hydroxylated-benzothiazine derivatives. DP1 with [M-H$^-$] at 170.0282 was identified as N-methyl-benzenesulfonamide. The above results compare well with previous advanced oxidation studies of PRX [18]. Finally, DP7 was assigned to methylated-PRX as a result of either an impurity in the initial PRX used or by the reaction of PRX with later stage products. By taking into account the above-identified DPs, the photocatalytic degradation pathways of PRX can be proposed (Figure 6). Regarding probable mechanisms, the first steps of degradation took place via hydroxyl radical attack on the PRX molecule leading to the formation of hydroxylated derivatives (DP 5,6,8). In parallel or consecutively, •OH radical attack on the carbonyl group gives rise to the hydrolytic cleavage of the amide bond via an addition-elimination reaction and a subsequent decarboxylation step results in the formation of hydroxylated-benzothiazine derivatives (DPs 2–4). A continuous •OH radical attack to the above intermediates resulted in the opening of the thiazine moiety and to the formation of N-methyl-benzenesulfonamide (DP1).

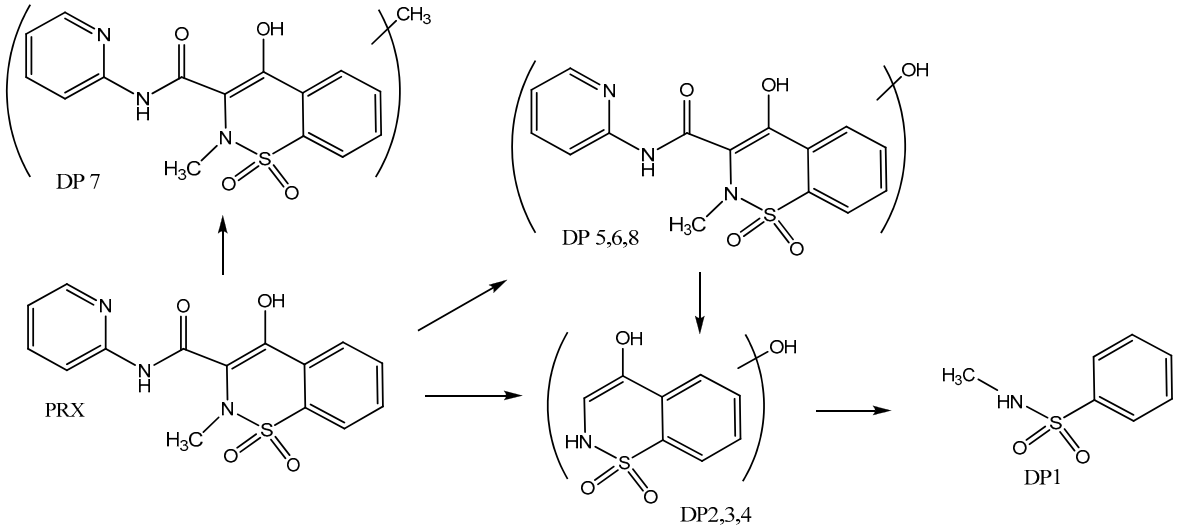


Figure 6. Photocatalytic degradation pathway of piroxicam.

Regarding the photoelectrocatalysis process, only DP1 and DP7 were identified at the time of sampling, while a light-green precipitate was formed progressively but mainly at the end of the treatment process. The precipitate was recovered after centrifugation, then dissolved in methanol and finally analyzed by LC-MS/MS. The chromatogram showed overlapped peaks at R_t = 16.00–17.00 with m/z 429.1842, 499.2629, and 605.2857. On the basis of the monitored molecular weights, coupling products of PRX with DPs can be suggested, however, no probable structures could feasibly be assigned. Further treatment times could lead to later stage products such as maleic, malonic, oxamic, glyoxylic acids, and finally acetic and oxalic acids as reported elsewhere for the electrooxidation of PRX [23].

3. Materials and Methods

3.1. Materials

Unless otherwise specified, reagents were obtained from Sigma Aldrich and were used as received. Millipore water was used in all experiments. SnO_2:F transparent conductive electrodes (FTO, Resistance 8 ohm/square) were purchased from Pilkington, USA. Glass plates employed in some cases as photocatalyst support were commercial microscope slides.

3.2. Deposition of the Titania Nanoparticulate Film

Nanoparticulate titania films were deposited on glass slides or FTO transparent electrodes by following protocols established by previous publications [24]. Briefly, the slide was cut in the appropriate dimensions and was carefully cleaned first with soap and then by sonication in isopropanol, water and acetone. A thin layer of compact titania was first sprayed over a patterned area using 0.2 mol L^{-1} diisopropoxytitanium bis(acetylacetonate) solution in ethanol and was calcined at 500 °C. Deposition of this bottom compact layer is a common practice with nanocrystalline titania films, since it enhances attachment of the top thick film, and in the case of electrodes, prevents short circuits and facilitates electron flow towards the electrode. On the top of this compact film, we applied a titania paste made of P25 nanoparticles by doctor blading. The film was calcined up to 550 °C at a rate of 20 °C/min. The final thickness of the film, as measured by SEM, was approximately 10 µm. The active geometrical area of the film was 2.5 × 5 cm and the mass of the catalyst was approximately 20 mg.

3.3. Description of the Reactor

Photocatalytic and photoelectrocatalytic degradation were carried out in a cylindrical batch reactor made of pyrex glass capable of accommodating a photoanode, counter, and reference electrode.

The photoanode was constructed with an FTO glass where nanoparticulate titania P25 was deposited, making an active surface film of 2.5 × 5 cm. The mass of the titania film was approximately 20 mg. The counter electrode was a Pt sheet of size 2.5 × 2.5 cm, while Ag/AgCl was used as reference electrode. The reactor was filled with a solution of the organic agent also containing 0.5 M Na_2SO_4 as supporting electrolyte and was operated by connection to a potentiostat [3]. For photocatalytic degradation, the photocatalyst was deposited on either a plain glass slide or an FTO glass. The size of the photocatalyst film and its total mass were the same, i.e., 2.5 × 5 cm active surface and 20 mg, respectively. Thus, the quantity of the photocatalyst and its active surface was the same in all cases studied. For photocatalytic degradation, FTO was not connected to any electrodes but it stood alone. Plain glass or FTO were always placed in a vertical position.

Illumination of the photocatalyst was produced with a low intensity black-light radiation in order to achieve a slow and controllable degradation process. The nominal power of the black-light tubes was 4W and the intensity of the incident radiation was approximately 1.5 mW cm^{-2} at the position of the photocatalyst film (measured with an ORIEL 70260 Radiant Power meter). In order to achieve this radiation level, four tubes were vertically symmetrically placed around the cylindrical reactor. The distance of each tube from the cylinder axis was approximately 6 cm and the reactor radius was 3 cm. Black Light-light radiation peaks in UVA and so it is ideal for exciting titania. No cooling of the reactor was necessary, thanks to the low intensity radiation level. The discoloration of the solution was monitored in all cases by absorption spectrophotometry for an irradiation period of 21–23 h. Prior to measurements, photocatalyst film was immersed in the solution for half an hour in the dark to reach dye-adsorption equilibrium.

3.4. Measurements and Characterizations

Absorption measurements were made with the help of a Cary 1E UV-Vis spectrophotometer (Houston, TX, USA) and application of an electric bias with an Autolab potentiostat PGSTAT128N (Utrecht, The Netherlands). In some experiments, Piroxicam degradation was also studied with High performance liquid chromatography according to our previous work [18]. Briefly, we used a Water Alliance 2695 separations module (Millford, DE, USA). The column used was a Kinetex (Phenomenex, Torrance, CA, USA) C18 100A (dimensions: 2.1 * 150 mm and 2.6 μm). The column was connected with an in line stainless steel filter 0.5 μm. (KrudKatcher Ultra) also purchased from Phenomenex, USA. The mobile phase was 32:68 acetonitrile and water and the flow rate 0.35 mL/min. The temperature maintained stable at 45 °C. The absorbance of Piroxicam was measured using a photodiode array detector (Waters 2996 PDA, Milford, MA, USA) at 350 nm.

LC-MS analysis was made as follows. An UPLC–ESI-MS/MS system including an Accela Autosampler, an Accela LC pump and a LTQ-Orbitrap mass spectrometer (Thermo Fisher Scientific, Germering, Germany) was used for the characterization of degradation products of Piroxicam. The chromatographic separations were run on a C18 Hypersil Gold, 100 × 2.1 mm i.d., 1.9 μm particle size (Thermo Fisher Scientific, San Jose, CA, USA), thermostated at 30 °C. Injection volume was 10 μL and flow rate 300 μL min^{-1}. Gradient mobile phase composition was adopted using water/5 mM ammonium formate as solvent A and methanol/5 mM ammonium formate as solvent B with the following program: 95/5 (1 min) to 5/95 in 15 min, and 95/5 in 22 min (holding for 1 min). Scan range was set between m/z 100–650 amu and for the sample pertain to the dissolved green precipitate formed during electrocatalysis was set at m/z 100–1000 amu. Prior to analysis, the orbitrap mass analyzer was externally calibrated to obtain mass accuracy with ±5 ppm. The analysis was performed using a resolving power of 60.000. UPLC–ESI/MS system was controlled with Xcalibur software version 2.1. All data (chemical formulae, mass accuracy and ring-double bond (RDB) equivalent values) were processed using also Xcalibur software. Mass accuracy of recorded ions was ±5 ppm units.

4. Conclusions

The main finding of this work is that deposition of nanoparticulate titania on FTO electrodes facilitated both BB41 and Piroxicam degradation with respect to the photocatalytic degradation obtained by depositing the same photocatalyst on plain glass. This was explained by the fact that FTO electrochemical potential is approximately 0.2 V, more positive than that of the conduction band of titania, therefore, injection of photogenerated electrons from titania to FTO is facilitated, thus encouraging electron-hole separation. When an electric bias was additionally applied, the photodegradation rate became even faster owing to enhanced electron-hole separation.

Author Contributions: I.P., G.K., and Z.F. Investigation. I.K., G.A. and D.M. Formal Analysis. P.L. Conceptualization.

Funding: This research received no external funding.

Acknowledgments: The authors wish to thank the unit of environmental, organic and biochemical high resolution-Orbitrap-LC-MS analysis of the University of Ioannina for providing access to the instrument facilities.

Conflicts of Interest: The authors declare no conflict of interest.

References

1. Bessegato, G.G.; Guaraldo, T.T.; de Brito, J.F.; Brugnera, M.F.; Zanoni, M.V.B. Achievements and Trends in Photoelectrocatalysis: From Environmental to Energy Applications. *Electrocatalysis* **2015**, *6*, 415–441. [CrossRef]
2. Ge, M.Z.; Cao, C.Y.; Huang, J.Y.; Li, S.H.; Zang, S.N.; Deng, S.; Li, Q.S.; Zhang, K.Q.; Lai, Y.K. Synthesis, modification, and photo/photoelectrocatalytic degradation applications of TiO_2 nanotube arrays: A review. *Nanotechnol. Rev.* **2016**, *5*, 75–112. [CrossRef]
3. Tantis, I.; Stathatos, E.; Mantzavinos, D.; Lianos, P. Photoelectrocatalytic degradation of potential water pollutants in the presence of NaCl using nanocrystalline titania films. *J. Chem. Technol. Biotechnol.* **2015**, *90*, 1338–1344. [CrossRef]
4. Qiu, L.; Wang, Q.; Liu, Z.; Zhao, Q.; Tian, X.; Li, H.; Gao, S. Preparation of 3D TiO_2 nanotube arrays photoelectrode on Ti mesh for photoelectric conversion and photoelectrocatalytic removal of pollutant. *Sep. Purif. Technol.* **2018**, *207*, 206–212. [CrossRef]
5. Paul, K.K.; Sreekanth, N.; Biroju, R.K.; Narayanan, T.N.; Giri, P.K. Solar light driven photoelectrocatalytic hydrogen evolution and dye degradation by metal-free few-layer MoS2 nanoflower/TiO_2(B) nanobelts heterostructure. *Sol. Energy Mater. Sol. Cells* **2018**, *185*, 364–374. [CrossRef]
6. Zhang, A.; Zhou, M.; Liu, L.; Wang, W.; Jiao, Y.; Zhou, Q. A novel photoelectrocatalytic system for organic contaminant degradation on a TiO_2 nanotube (TNT)/Ti electrode. *Electrochim. Acta* **2010**, *55*, 5091–5099. [CrossRef]
7. Turolla, A.; Bestetti, M.; Antonelli, M. Optimization of heterogeneous photoelectrocatalysis on nanotubular TiO_2 electrodes: Reactor configuration and kinetic modeling. *Chem. Eng. Sci.* **2018**, *182*, 171–179. [CrossRef]
8. Strataki, N.; Bekiari, V.; Stathatos, E.; Lianos, P. Effect of aggregation of dyes adsorbed on nanocrystalline titania films on the efficiency of photodegradation. *J. Photochem. Photobiol. A Chem.* **2007**, *191*, 13–18. [CrossRef]
9. Tantis, I.; Bousiakou, L.; Frontistis, Z.; Mantzavinos, D.; Konstantinou, I.; Antonopoulou, M.; Katrikase, G.A.; Lianos, P. Photocatalytic and photoelectrocatalytic degradation of the drugomeprazole on nanocrystalline titania films in alkaline media: Effect of applied electrical bias on degradation and transformation products. *J. Hazard. Mater.* **2015**, *294*, 57–63. [CrossRef] [PubMed]
10. Peleyeju, M.G.; Umukoro, E.H.; Tshwenya, L.; Moutloali, R.; Babalola, J.O.; Arotiba, O.A. Photoelectrocatalytic water treatment systems: Degradation, kinetics and intermediate products studies of sulfamethoxazole on a TiO_2–exfoliated graphite electrode. *RSC Adv.* **2017**, *7*, 40571–40580. [CrossRef]
11. Ghasemian, S.; Nasuhoglu, D.; Omanovic, S.; Yargeau, V. Photoelectrocatalytic degradation of pharmaceutical carbamazepine using Sb-doped $Sn_{80\%}$-$W_{20\%}$-oxide electrodes. *Sep. Purif. Technol.* **2017**, *188*, 52–59. [CrossRef]
12. Janssens, R.; Mandal, M.K.; Dubey, K.K.; Luis, P. Slurry photocatalytic membrane reactor technology for removal of pharmaceutical compounds from wastewater: Towards cytostatic drug elimination. *Sci. Total Environ.* **2017**, *599–600*, 612–626. [CrossRef] [PubMed]

13. Serpone, N.; Artemev, Y.M.; Ryabchuk, V.K.; Emeline, A.V.; Horikoshi, S. Light-driven advanced oxidation processes in the disposal of emerging pharmaceutical contaminants in aqueous media: A brief review. *Curr. Opin. Green Sustain. Chem.* **2017**, *6*, 18–33. [CrossRef]
14. Stathatos, E.; Papoulis, D.; Aggelopoulos, C.A.; Panagiotaras, D.; Nikolopoulou, A. TiO_2/palygorskite composite nanocrystalline films prepared by surfactant templating route: Synergistic effect to the photocatalytic degradation of an azo-dye in water. *J. Hazard. Mater.* **2012**, *211–212*, 68–76. [CrossRef] [PubMed]
15. Apostolopoulou, A.; Mahajan, S.; Sharma, R.; Stathatos, E. Novel development of nanocrystalline kesterite Cu_2ZnSnS_4 thin film with high photocatalytic activity under visible light illumination. *J. Phys. Chem. Solids* **2018**, *112*, 37–42. [CrossRef]
16. Mahmoodi, N.M.; Abdi, J.; Oveisi, M.; Asli, M.A.; Vossoughi, M. Metal-organic framework (MIL-100 (Fe)): Synthesis, detailed photocatalytic dye degradation ability in colored textile wastewater and recycling. *Mater. Res. Bull.* **2018**, *100*, 357–366. [CrossRef]
17. Bouras, P.; Lianos, P. Photodegradation of dyes in aqueous solutions catalyzed by highly efficient nanocrystalline Titania films. *J. Appl. Electrochem.* **2005**, *35*, 831–836. [CrossRef]
18. Lianou, A.; Frontistis, Z.; Chatzisymeon, E.; Antonopoulou, M.; Konstantinou, I.; Mantzavinos, D. Sonochemical oxidation of piroxicam drug: Effect of key operating parameters and degradation pathways. *J. Chem. Technol. Biotechnol.* **2018**, *93*, 28–34. [CrossRef]
19. Bacsi, I.; Beres, V.B.; Kokai, Z.; Gonda, S.; Novak, Z.; Nagy, S.A.; Vasas, G. Effects of non-steroidal anti-inflammatory drugs on cyanobacteria and algae in laboratory strains and in natural algal assemblages. *Environ. Pollut.* **2016**, *212*, 508–518. [CrossRef] [PubMed]
20. Ziylan, A.; Ince, N.H. The occurrence and fate of anti-inflammatory and analgesic pharmaceuticals in sewage and fresh water: Treatability by conventional and non-conventional processes. *J. Hazard. Mater.* **2011**, *187*, 24–36. [CrossRef] [PubMed]
21. Motoyoshi, R.; Oku, T.; Suzuki, A.; Kikuchi, K.; Kikuchi, S.; Jeyadevan, B.; Cuya, J. Fabrication and Characterization of Copper System Compound Semiconductor Solar Cells. *Adv. Mater. Sci. Eng.* **2010**, *2010*, 562842. [CrossRef]
22. Pop, L.C.; Drakopoulos, V.; Lianos, P. Photoelectrocatalytic hydrogen production using nanoparticulatetitania and a novel Pt/carbon electrocatalyst: The concept of the "Photoelectrocatalytic Leaf". *Appl. Surf. Sci.* **2015**, *333*, 147–151. [CrossRef]
23. Feng, L. Advanced Oxidation Processes for the Removal of Residual Non-Steroidal Anti-Inflammatory Pharmaceuticals from Aqueous Systems. Ph.D. Thesis, Earth Sciences, Université Paris-Est, Marne-la-Vallée, France, 2013. (In English)
24. Doukas, E.; Balta, P.; Raptis, D.; Avgouropoulos, G.; Lianos, P. A Realistic Approach for Photoelectrochemical Hydrogen Production. *Materials* **2018**, *11*, 1269. [CrossRef] [PubMed]



© 2018 by the authors. Licensee MDPI, Basel, Switzerland. This article is an open access article distributed under the terms and conditions of the Creative Commons Attribution (CC BY) license (http://creativecommons.org/licenses/by/4.0/).